Loss of VPS41 triggers rapid insulin degradation and dysregulated autophagy in pancreatic beta cells

Short running title: VPS41 loss causes insulin degradation in beta-cells

Yau B[1]*, An Y[1]*, Germanos M[1], Schwarzkopf P[1], van der Kraan G[1], Larance M[1], Burns C[2], Asensio CS[2], Kebede MA[1#]

[1]School of Medical Sciences, Charles Perkins Centre, The University of Sydney, Camperdown, New South Wales, Australia

[2]Department of Biological Sciences, University of Denver, Denver, CO

*These authors contributed equally.

#Corresponding author: melkam.kebede@sydney.edu.au, +61 2 8627 0164

Word count: 4736, Figures: 7

Abstract

Vacuolar protein sorting-associated protein 41 (VPS41) has previously been established as a requirement for normal insulin secretory function in pancreatic beta-cells, with genetic deletion of VPS41 in insulinoma cells (VPS41KO) resulting in defects in insulin granule composition and secretory behaviour. In mice, VPS41 deletion in pancreatic beta-cells presented as severe hyperglycaemia due to an insulin insufficiency. Presently, we show that chronic VPS41 deletion modeled in VPS41KO insulinoma cells and aged VPS41 beta-cell knockout mice results in beta-cell dedifferentiation associated with downregulation of beta-cell identity genes and insulin granule pathway proteins. In mice, a sexually dimorphic response to beta-cell specific VPS41 deletion is observed, with young female mice exhibiting preserved insulin content, less upregulation of degradation pathway-associated proteins, and reduced ER stress, compared to young male mice. In an acute model of VPS41 depletion *in vitro*, VPS41-dependent loss of insulin is associated with cytosolic redistribution of mammalian target of rapamycin (mTOR), increased nuclear localisation of transcription factor E3, and impaired autophagy in VPS41KD cells. Inhibition of lysosomal degradation with chloroquine or a cysteine protease inhibitor rescues the rapidly depleted insulin content. This phenotype reflects a HOPS-dependent mechanism for insulin content regulation, with VPS41 functioning as a critical component.

Article Highlights

Why did we undertake this study?

VPS41 deletion causes insulin loss in beta-cells through an unknown mechanism.

What is the specific question we wanted to answer?

How does VPS41 regulate insulin content in beta-cells?

36 *What did we find?*

37 Acute VPS41 depletion impairs the autophagolysosomal pathway while chronic VPS41
38 deletion down-regulates beta-cell identity. VPS41-dependent loss of insulin content is sexually
39 dimorphic.

40 *What are the implications of our findings?*

41 VPS41 mutations exist in humans and VPS41-dependent regulation of insulin content has
42 implications for diabetes susceptibility. Understanding how insulin degradation dysregulates is
43 essential to the development of beta-cell targeting therapies to preserve insulin.

44 **(Introduction)**

45 Regulation of insulin content in pancreatic beta-cells is at the core of beta-cell function. It relies
46 on a carefully curated balance between insulin secretory granule (ISG) biosynthesis, storage,
47 degradation, and secretion[1]. In conditions of glucose abundance when more insulin secretion
48 is required, insulin degradation is decreased[2] and insulin synthesis is increased [3];
49 characterised in the beta-cell by enhanced insulin promoter activation, elevated INS1 gene
50 expression [3], and expansion of the endoplasmic reticulum and Golgi apparatus to
51 accommodate increased ISG formation[4]. Intracellular ISG storage is also higher, reflected in
52 increased beta-cell mass[4]. On the contrary, in conditions of reduced secretory need, ISG
53 synthesis is downregulated, and insulin storage is minimized. Insulin granule degradation to
54 control insulin content is mediated through multiple cellular pathways; crinophagy – direct
55 insulin granule to lysosome fusion to degrade granule contents[5], conventional
56 macroautophagy – in which insulin granules are contained within autophagosomal bodies for
57 lysosomal fusion – or microautophagy[6] – in which insulin granules are autophagocytosed by
58 the lysosomal compartment, also appear to contribute to insulin granule turnover[7]. There also

59 exist specialized pathways to degrade ISGs known as stress/starvation-induced nascent granule
60 degradation (SINGD), which are activated to preserve cellular resources[8, 9].

61 Vacuolar protein sorting-associated protein 41 (VPS41) is a core component of the homotypic
62 fusion and vacuole protein sorting (HOPS) tethering complex, which functions as a mediator
63 of vesicle fusion between intracellular degradative compartments of the cell[10-12].
64 Independent of the HOPS complex, VPS41 has additional roles in protein trafficking between
65 vacuolar compartments such as the lysosome and endosome through interactions with
66 Rab7[13], Adapter Protein 3 (AP3)[14, 15] and Rab5[16], though some of these pathways have
67 yet to be verified in mammalian cells. More recently, a role for VPS41 the regulated secretory
68 pathway has been identified, implicating the protein in granule biogenesis for the first time[14].

69 Human VPS41 mutations have recently been characterised[17], with these extending to
70 clinically relevant single nucleotide polymorphisms (SNPs) in VPS41 causing
71 neurodegenerative pathologies in human families[18]. Inherited biallelic loss of function
72 VPS41 variants have also been evidenced to cause progressive dystonia and cerebellar
73 dysfunction in patients, with implications for impaired lysosomal function[18, 19].
74 Importantly, these neuropathologies appear to be driven by dysfunction of the HOPS complex,
75 in which a VPS41 mutation results in a HOPS loss of function phenotype.

76 In pancreatic beta-cells, VPS41 deletion and SNPs exhibited similar phenotypes to those
77 described in the brain[17, 20]. Dissolution of HOPS complex function by either VPS41 or
78 VPS39 – another core component of HOPS – depletion results in impaired endolysosomal
79 fusion, and consequently defective cargo degradation[20]. Importantly, our initial study in
80 insulinoma INS1 beta-cells established the existence of a separate pool of HOPS-independent
81 VPS41 protein that also contributes to ISG biogenesis, and this VPS41 pool remained stable
82 despite HOPS destabilization when VPS39 alone was depleted. We showed significant changes

83 to insulin granule morphology and composition occurs in CRISPR-Cas9-generated VPS41
84 knockout beta-cells[20], building on prior findings that VPS41 may exert a role as a coat
85 protein for granule formation[14]. Most strikingly, a S284P single nucleotide polymorphism in
86 VPS41 was sufficient to disrupt HOPS while keeping VPS41's function in the insulin secretory
87 pathway intact, suggesting that VPS41 has both HOPS-dependent and -independent functions
88 in the beta-cell. Importantly, we also determined that *in vivo* genetic deletion of VPS41
89 specifically in beta-cells using the *Ins1-Cre* transgenic mouse line resulted in an insulin-
90 sensitive diabetic phenotype in mice, characterised by insulin insufficiency and extreme
91 hyperglycaemia[20]. These findings were a crucial step in defining the relationship between
92 VPS41 and the insulin secretory pathway.

93 In our present study we disentangle the acute and chronic effect of VPS41 deletion in pancreatic
94 beta-cells using an siRNA-mediated knockdown of VPS41 in insulinoma cells (VPS41KD),
95 and the characterisation of young VPS41KO mice. We establish a sexually dimorphic response
96 to VPS41 deletion-driven insulin loss through differences in female susceptibility to ER-stress-
97 associated autophagy and determine that mature insulin granules are rapidly degraded in
98 VPS41KD cells through lysosomal degradation despite disruptions to autophagolysosomal
99 fusion. These data represent the critical nature of HOPS-dependent VPS41 function in beta-
100 cells.

101 **Research Design and Methods**

102 *Cells*

103 INS-1 cells (gifted from Dr. Peter Arvan, University of Michigan, Ann Arbor, MI) were
104 maintained in RPMI (with 10% FBS, 1 mmol/L sodium pyruvate, 50 μmol beta-
105 mercaptoethanol, 1% penicillin-streptomycin) at 5% CO_2 and 37°C. VPS41KO cells were
106 generated as previously described[20].

107 *Plasmids*

108 VPS41 siRNA for knockdown experiments was commercially generated (Thermo Fisher
109 Silencer Select siRNAs) using siRNA Assay ID s157874, alongside Silencer Select Negative
110 Control No.1 (4390843). proinsulin-msGFP2 was generated from pQE-60NA-proinsulin-
111 msGFP2 (Addgene, #160466) and verified by Sanger sequencing (Garvan Molecular Genetics,
112 Australia).

113 *Degradation Inhibition*

114 Chloroquine (C6628), MG132 (M8699), E64D (E3132) and ammonium chloride (326372)
115 were all obtained from Sigma-Aldrich.

116 *Mass spectrometry-based proteomics*

117 Protein samples for bottom-up proteomics analysis were prepared as describe previously[21].
118 Briefly, proteins were extracted in a buffer containing 4% sodium deoxycholate (SDC), 40 mM
119 chloroacetamide, 10 mM TCEP and 0.1 M Tris-HCl (pH 8.0) in water. Samples were then
120 incubated at 95°C for 10 min at 1000 rpm in a Thermomixer-C (Eppendorf). Samples were
121 diluted to a final concentration of 1% SDC with water and 10 ug of protein digested overnight
122 with 200 ng of MS-grade trypsin (Sigma) in 50 mM acetic acid at 37°C, on a Thermomixer-C
123 (Eppendorf) at 1000 rpm. Samples were mixed with ethyl acetate (50% final concentration,
124 v/v), vortexed until SDC precipitates dissolved. SDB-RPS StageTips were prepared, sample
125 purification performed as described previously[21]. Peptides were reconstituted with 5 %
126 formic acid in MS-grade H2O, sealed and stored at 4 °C until LC-MS/MS acquisition.

127 Using a ThermoFisher RSLCnano ultrahigh performance liquid chromatograph, peptides in 5
128 % (v/v) formic acid (3 µL injection volume) were injected onto a 50 cm x 75 µm C18Aq (Dr
129 Maisch; 1.9 µm) fused analytical column with a ~10 µm pulled tip, coupled online to a
130 nanospray electrospray ionization source. Peptides were resolved over gradient from 5 – 40 %

131 acetonitrile for 70 min, with a flow rate of 300 nL min-1 (Capillary flow). Electrospray
132 ionization was done at 2.3 kV. Tandem mass spectrometry analysis was carried out on a
133 Exploris or Lumos Tribrid mass spectrometer (ThermoFisher) using data-independent
134 acquisition (DIA). DIA was performed as previously described using variable isolation widths
135 for different m/z ranges 114. Stepped normalized collision energy of 25 ± 10 % was used for
136 all DIA spectral acquisitions.

137 Raw MS data were analyzed using quantitative DIA proteomics software DIA-NN (v. 1.8).
138 Complete mouse proteome databased from UNIPROT was used for neural network generation,
139 with deep spectral prediction enabled. Protease digestion was set to trypsin (fully specific)
140 allowing for two missed cleavages and one variable modification. Oxidation of Met and
141 acetylation of the protein N-terminus were set as variable modifications. Carbamidomethyl on
142 Cys was set as a fixed modification. Match between runs and remove likely interferences were
143 enabled. Neural network classifier was set to double-pass mode. Protein interferences were
144 based on genes. Quantification strategy was set to any liquid chromatography (LC, high
145 accuracy). Cross-run normalization was set to RT-dependent. Library profiling was set to smart
146 profiling.

147 *Mice*

148 Ins1-Cre control (CTRL), and beta-cell specific VPS41 heterozygous (VPS41HET) and
149 homozygous (VPS41KO) mice were bred at Australian BioResources (Garvan institute of
150 Medical Research) and transferred to the Charles Perkins Centre (The University of Sydney)
151 for experimental procedures. Mice were fed a standard laboratory chow (13% calories from
152 fat, 65% carbohydrate, and 22% protein) from Gordon's Specialty Stock Feeds (Yanderra, New
153 South Wales, Australia). VPS41*fl/fl* mice (26) were crossed with Ins1-Cre mice (strain 026801;
154 The Jackson Laboratory) to generate third generation VPS41*fl/fl*, VPS41*fl/*+ and *Ins1-cre*/+

155 mice and their littermate controls for experiments. Male and female mice were used where
156 indicated. Mice were maintained on a 12-h light/dark cycle (0700/1900 h) with *ad libitum*
157 access to food and water. Experiments were carried out in accordance with the National Health
158 and Medical Research Council (Australia) guidelines for animal research and approved by The
159 University of Sydney Animal Experimentation Ethics Committees (Camperdown, New South
160 Wales, Australia).

161 *Mouse metabolic phenotyping*

162 Magnetic resonance imaging (MRI) was conducted (EchoMRI 900) to determine lean and fat
163 mass and mice were administered glucose (2 g / kg lean mass) by oral gavage. Mice were fasted
164 for 5 hours prior to oral-GTT. Blood glucose was measured immediately prior to and 15, 30,
165 45, 60 and 90 min after glucose injection with ACCU-CHEK Performa II Strips (Roche, Basel,
166 CH). Blood was collected immediately prior to and 15 minutes after glucose injection for
167 plasma insulin measurements.

168 *Islet Isolation and Glucose-induced insulin secretion assays*

169 Islets were harvested from mice as previously described[22]. Glucose-induced insulin secretion
170 assays were performed in isolated islets as previously described[22]; islets were placed into 2.8
171 mM glucose Krebs Ringer buffer supplemented with 10 mM HEPES (KRBH) for 1 hour prior
172 to assay as pre-basal. New KRBH media containing 2.8 mM was added, then collected after 1
173 hour (basal secretion). Islets were then stimulated with KRBH containing 16.7 mM glucose
174 and supernatant collected after 1 hour (stimulated secretion). Islets were then washed in PBS
175 and lysed by sonication in Islet Lysis Buffer (100mM Tris pH7.4, 300mM NaCl, 10mM NaF)
176 to measure total islet insulin content.

177 *Insulin measurements*

178 Plasma insulin measurements were obtained using an Ultra-Sensitive Insulin ELISA Assay
179 (Crystal Chem). *Ex vivo* islet and INS1 cell glucose-stimulated insulin secretion assay insulin
180 measurements were obtained using a rapid homogenous time-resolved fluorescence (HTRF)
181 Insulin Assay kit (Cisbio Assay).

182 *Immunofluorescent staining*

183 Paraffin-embedded pancreas tissue was processed as previously described [20].
184 Immunofluorescent staining for proinsulin, insulin, mTORC1, TFE3 was performed as
185 previously described[23]. Pancreas slices and cell coverslips were washed and mounted with
186 ProLong Diamond Antifade (Invitrogen).

187 *SDS-PAGE*

188 Proteins in whole-cell lysates and fractions were separated using MES buffer SDS-PAGE
189 under denaturing conditions on 4 - 12% Bis-Tris Bolt^{TM} polyacrylamide gels (Invitrogen), then
190 transferred to methanol-activated PVDF membranes. The modified Western blotting method
191 recently described by Okita et al.[24] was used to immunoblot for proinsulin and insulin.

192 *Antibodies*

193 The following commercial antibodies and their sources are listed: VPS41 (sc-377118, SCBT),
194 LC3A/B (12741, CST), LAMP1 (ab24170, Abcam), Insulin (IR00261-2, Agilent DAKO),
195 Proinsulin (GS-9A8, DSHB), Chromogranin A (NB120-15160SS, Novus Biologicals), Rab5
196 (3547, CST), Beta-actin (A5441, Sigma), phospho-eIF2a (3398, CST), total-eIF2a (5324,
197 CST), phospho-IRE1-alpha (PA1-16927, Invitrogen), total IRE1-alpha (3298, CST), Beclin-1
198 (3495, CST), Atg12 (4180, CST), CHOP (2895, CST), BiP/GRP78 (3177, CST), phospho-JNK
199 (4668, CST), total-JNK (67096, CST), mTORC1 (2983, CST), TFE3 (MA537818, Invitrogen).

200 *Analysis and Statistics*

201 Immunofluorescence image analysis for fluorescence intensity, colocalisation and western blot
202 quantification was performed in FIJI (Image J). Proteomic analysis was performed in Perseus
203 (v1.6.15 MaxQuant). Statistical analyses were performed in Prism (GraphPad Prism 8).

204 **Results**

205 **Chronic VPS41 deletion results in loss of beta-cell identity.** VPS41KO INS1 cells,
206 previously generated using CRISPR Cas9[20], were subject to mass spectrometry-based
207 proteomics to determine global protein changes. Following MS validation and normalization
208 (see Methods), we identified 1100 differentially expressed proteins – 658 downregulated and
209 442 upregulated – in VPS41KO INS1 beta-cells (Figure 1A). GO pathway analysis identified
210 processes associated with *RNA splicing*, *nucleic acid processing*, and *regulation of gene*
211 *expression* in upregulated proteins, and *lipid metabolic processes*, and *regulation of secretion*
212 *and peptides* in downregulated proteins (Figure 1B). Downregulated proteins included insulin
213 (INS1), glucokinase (GCK), insulin secretory pathway-associated proteins such as the
214 prohormone convertases (PCSK1, PCSK2) and chromogranins (CHGA, CHGB), as well as the
215 classic beta-cell identity marker insulin promoter factor 1 (PDX1) (Figure 1C). Significantly,
216 upregulated proteins included hexokinases (HK1, HK2), lactase dehydrogenase A (LDHA) and
217 aldehyde dehydrogenase (ALDH1B1), which are conventional beta-cell "disallowed" genes
218 associated with beta-cell dedifferentiation[25] (Figure 1D).

219 In an attempt to rescue insulin content in VPS41KO cells, we transfected WT INS1 and
220 VPS41KO INS1 cells with a GFP-tagged proinsulin DNA construct (Figure 1E). While
221 proinsulin-GFP expression was readily visualised in a perinuclear region colocalizing with
222 immunofluorescent (pro)insulin staining in WT INS1 cells, VPS41KO INS1 cells failed to
223 express the proinsulin-GFP construct (Figure 1E), further suggesting a loss of beta-cell identity

224 extending to proteins involved in proinsulin synthesis. Reduced (pro)insulin staining in
225 VPS41KO cells was consistent with that previously observed in these cells[20].

226 Previously, VPS41 beta-cell specific KO mice were characterised at 16 weeks age[20],
227 establishing a severe loss of insulin content and insulin secretory capacity in these mice,
228 resulting in significantly high blood glucose levels with no changes in insulin sensitivity.
229 Presently, we compared blood glucose concentrations of 6-week and 16-week-old female Cre
230 control (CTRL), VPS41 beta-cell heterozygous (VPS41HET) and VPS41 beta-cell knock out
231 (VPS41KO) mice, showing an age-dependent loss of glucose homeostasis in VPS41KO mice
232 only (Figure 2A). Proteomic analysis of VPS41HET and VPS41KO islets from these mice also
233 demonstrated progressive, age-dependent changes to the islet proteome, with 11% of the islet
234 proteome changed (761 differentially expressed) in 6-week-old VPS41KO mice compared to
235 VPS41HET, but 43% of the islet proteome altered (3084 differentially expressed) in 16-week-
236 old VPS41KO mice compared to VPS41HET (Figure 2B). When we performed GO pathway
237 analysis on differentially expressed pathways, we identified upregulated pathways at 6 weeks
238 that persisted to 16 weeks included *macroautophagy*, *lytic vacuole organisation* and *lysosomal*
239 *transport*, while downregulated pathways at 6 weeks that persisted to 16 weeks included
240 *regulation of gene expression, negative regulation of RNA processing* and *chromatin assembly*
241 (Figure 2C). Significantly, in islets of 16-week-old mice, we observed downregulation of
242 granule proteins such as neuropeptide Y (NPY) and secretogranin (SCGN), and upregulation
243 of lysosomal proteins (LAMP1, LAMP2), insulin degrading enzyme 1 (IDE1) and cathepsins
244 (CTSL, CTSD, Figure 1D). Finally, we found that while insulin (INS1, INS2) was not changed
245 at 6-weeks, it was significantly downregulated by 16-weeks, and this was preceded by
246 downregulation of insulin promotor factor 1 (PDX1) (Figure 1E). Altogether these data provide
247 strong evidence for progressive changes to beta-cell function and identity due to chronic
248 deletion of VPS41, potentially through downregulation of PDX1.

249 **Acute loss of mature insulin in VPS41 depletion mirrors VPS41 KO prior to loss of beta-**
250 **cell identity.** To separate the effects of acute and chronic VPS41 deletion in beta-cells, we
251 established a VPS41 depletion model using siRNA-mediated VPS41 knockdown in WT INS1
252 cells (VPS41KD). Time-dependent depletion of VPS41 over a 72-hour timecourse resulted in
253 a corresponding depletion specifically of insulin granules as measured by insulin and
254 chromogranin A (CgA), with no apparent changes to lysosomes (LAMP1) or endosomes
255 (Rab5, Figure 3A). By 48 hours post-transfection, VPS41 expression levels were 22 %
256 compared to non-targeting transfection controls (Figure 3B). Insulin levels were 18 % of
257 controls when compared by SDS-PAGE immunoblotting (Figure 3C), and 47 % by
258 immunofluorescence intensity (Figure 3D).

259 Proteomic analysis of VPS41KD cells at 72 hours transfection identified 1677 proteins
260 differentially expressed compared to non-targeting siRNA controls (Figure 3E), with GO
261 pathway analysis identifying upregulated pathways in *protein phosphatase inhibitor activity*
262 and *enzyme inhibitor activity* (Figure 3F). Neither LAMP1 nor LAMP2 expression changed,
263 but the autophagosome marker sequestosome 1 (SQSTM1) was significantly upregulated in
264 VPS41KD cells. Interestingly, while there was no change to insulin (INS1), the prohormone
265 convertases (PCSK1, PCSK2) or chromogranin A (CHGA), chromogranin B (CHGB)
266 expression was decreased, and PDX1 expression was increased in VPS41KD cells (Figure 3G,
267 left). Additionally, no VPS41 expression was detected by mass spectrometry in our VPS41KD
268 cells, and notably, acute VPS41 depletion was sufficient to destabilise the HOPS complex, with
269 undetected expression of all core HOPS proteins (VPS11, VPS16, VPS18, VPS33a) (Figure
270 3G, right).

271 Finally, a glucose-stimulated insulin assay performed on VPS41KD cells at 72 hours post-
272 transfection revealed no secretory defect upon single glucose stimulus at 16.7 mM glucose

273 (Figure 3H), but a significant loss of insulin content (Figure 3I), suggesting acute VPS41
274 deletion initially exerts control over insulin stores, and not secretory function.

275 **Sexually dimorphic response to *in vivo* VPS41 deletion in the beta-cell is driven by**
276 **autophagy-ER stress susceptibility.** Sex-dependent differences to diabetic and glucose
277 phenotypes are previously documented[26, 27], however our initial characterisation of
278 VPS41KO mice were performed in a mixed-gender littermates[20]. Presently, we characterised
279 male and female VPS41KO mice and VPS41HET controls at 6 weeks age, where female
280 VPS41KO mice have now been described to retain insulin expression (Figure 2E). Body
281 composition of males and females were not different between genotypes (Figure 4A), but
282 fasting blood glucose levels were significantly increased in both male and female VPS41KO
283 mice compared to HET controls. Importantly, male VPS41KO mice displayed increased blood
284 glucose compared to female VPS41KO mice (Figure 4B), but there was no difference between
285 fasting insulin levels in mice of either sex or genotype (Figure 4C).

286 When an oral glucose tolerance test (oGTT) was performed, both male and female VPS41KO
287 mice exhibited impaired glucose tolerance (Figure 4D), but only male mice exhibited
288 significantly impaired insulin secretion in response to glucose (Figure 4E). There was an
289 increase in the oGTT area under the curve (AUC) of VPS41KO mice compared to VPS41HET
290 controls (Figure 4F) as well as between male and female VPS41KO mice (Figure 4F). Notably,
291 when expressing oGTT values as a percentage of baseline to account for elevated fasting
292 glucose levels in VPS41KO mice (Figure 4G), an impairment in glucose tolerance was revealed
293 in male VPS41KO only, as measured by incremental AUC, suggesting that female VPS41KO
294 mice remained glucose responsive despite increased fasting blood glucose levels (Figure 4H).

295 When islets were isolated to perform *ex vivo* glucose-stimulated insulin secretion, we found no
296 differences in basal (2.8 mM glucose) and stimulated (16.7 mM glucose) responses between

297 female VPS41KO mice and VPS41HET controls. Matching *in vivo* insulin responses during
298 the oGTT (Figure 4E), male VPS41KO mice exhibited impaired insulin secretion at 16.7 mM
299 glucose during glucose-stimulated insulin secretion (Figure 4I). Male VPS41KO mice also had
300 significantly reduced insulin content in their islets, which was not observed in female
301 VPS41KO mice (Figure 4J). Accordingly, when insulin secretion was expressed relative to
302 insulin content per islet, a lack of secretory response in male VPS41KO was readily apparent
303 (Figure 4K). Immunofluorescent staining in pancreatic tissue of male and female VPS41KO
304 mice also a clearly observed reduction in insulin fluorescence intensity in islets of male
305 VPS41KO mice (Figure 4L).

306 As estrogen exerts protective effects on the pancreatic beta-cell[28, 29], in some cases through
307 ER-stress protection[26], we performed ovariectomy (OVX) and sham (SHAM) procedures on
308 5-week-old female VPS41KO mice and VPS41HET controls to investigate this possibility.
309 Blood glucose levels were measured when mice were 8 weeks of age, and no significant
310 difference was observed between OVX and SHAM groups in the VPS41KO mice (Figure 4M).
311 Notably, blood glucose levels of female VPS41KO in the OVX group did not reach those
312 observed in male mice even at 6 weeks (Figure 4B), suggesting the protective effect we observe
313 in female mice is not solely estrogen dependent.

314 Finally, islets were isolated from male and female VPS41KO and VPS41HET mice at 7 weeks
315 age to assess protein expression (Figure 5A). VPS41 expression levels in VPS41KO were
316 validated in both male and female mice, with low levels of VPS41 in VPS41KO mice attributed
317 to alpha-cell-localised expression in islets. As autophagy and lysosomal activity were processes
318 identified in our proteomic analysis, we measured markers for lysosomes (LAMP1) and
319 autophagosomes (LC3A/B) and found increased LAMP1 and LC3A/B expression in both male
320 and female VPS41KO mice compared to VPS41HET controls. Importantly, we only observed

321 a significant difference in LC3A/B between male and female KO mice, exposing a sex-
322 dependent effect within the autophagy pathway (Figure 5B).

323 As endoplasmic stress (ER) is an established trigger for autophagy in pancreatic beta-cells[30,
324 31], we also examined expression of key ER stress markers in our islets. No differences were
325 observed in the levels of phosphorylated eIF2a, phosphorylated IRE1, Beclin-1, or Atg12
326 between VPS41KO mice and VPS41HET controls of either sex. However, expression of
327 BiP/GRP78 and phosphorylated JNK were significantly increased in male VPS41KO relative
328 to female VPS41KO mice, which exhibited levels similar to VPS41HET controls.
329 Interestingly, CHOP was increased in both male and female VPS41KO mice compared to
330 VPS41HET controls, with female VPS41KO trending towards higher expression than male
331 VPS41KO mice (Figure 5B).

332 In summary, these data strongly evidence a sex-dependent response to genetic deletion of
333 VPS41, with males showing increased loss of insulin content, likely through an ER-stress
334 associated autophagy pathway.

335 **VPS41-dependent loss of insulin is associated with cytosolic redistribution of mTORC1**
336 **and increased nuclear localisation of transcription factor E3.** Previous characterisation of
337 VPS41 deletion in neuroendocrine cells reported phenotypes indicating defective activation of
338 autophagy pathways; TFE3 nuclear translocation was observed concurrent with dissociation of
339 mTORC1 from the lysosome[17]. Presently, we report congruous findings in the INS1 cell line
340 at 24h post-VPS41 knockdown (Figures 6A and B). In VPS41KO INS1 cells, expression of
341 mCherry-eGFP-LC3 to visualise autophagic flux identified an autophagolysosomal fusion
342 delay (Supplemental Figure 1A), congruous with increased autophagosome cargo protein
343 SQSTM1 expression in VPS41KD cells (Figure 3G) and increased LC3 protein expression

344 observed in VPS41KO mouse islets (Figure 5A and B). Altogether these data expose a
345 regulatory role for VPS41 in the autophagolysosomal pathway of pancreatic beta-cells.

346 **VPS41 depletion triggers rapid lysosomal degradation of mature insulin granules.** VPS41
347 knockdown-driven insulin degradation at 24 hours post-transfection was not matched by
348 proinsulin degradation (Figure 6C), indicating selective loss of mature insulin granules
349 independent of changes to proinsulin synthesis. This was further evidenced by similar levels
350 of proinsulin staining in control and VPS41KD cells at 24 hours post-transfection (Figure 6D).
351 Differences in insulin were also not detected in the media of control and VPS41KD cells within
352 the first 24 hours of siRNA, indicating insulin was not redirected to constitutive secretion
353 (Figure 6E). In VPS41KD cells, an 18 hour pretreatment of INS1 cells with cysteine protease
354 inhibitor E64D and lysosomal inhibitor chloroquine, but not proteosome inhibitor MG132 or
355 ammonium chloride (Supplemental Figure 1B), was able to restore insulin levels to that of
356 control cells (Figure 6F and G), confirming the selective loss of mature insulin granules was
357 occurring through a lysosomal pathway.

---

358 **Discussion**

359 **VPS41 is indispensable to the beta-cell.** We first established the significance of VPS41 in
360 beta-cells in our characterisation of VPS41 INS1 KO cells and VPS41 beta-cell KO mice[20],
361 showing that genetic deletion of the VPS41 protein in beta-cells resulted in an impaired
362 glucose-stimulated secretory response and dramatic loss of total insulin content. In mice, this
363 translated to a unique diabetic phenotype defined by insulin insufficiency in the absence of
364 insulin resistance (or an immune response). Presently we aimed to extricate the effects of
365 chronic insulin deficiency from acute VPS41 depletion to better understand VPS41 function in
366 both *in vitro* and *in vivo* contexts.

367 It is apparent from our present data that VPS41 likely has dual functions within the insulin
368 secretory pathway in regulating both insulin secretion and insulin content; VPS41 is implicated
369 as a coat protein alongside AP-3 at early stages of insulin granule budding at the *trans*-Golgi
370 network[14], but as a component of the HOPS complex, mediates maintenance of insulin
371 granule storage. It also appears that there are no functional redundancies for VPS41; while
372 HOPS complex dissolution in VPS39 KD leaves an intact pool of VPS41 still capable of
373 regulating insulin secretion[20], deletion of full length VPS41 is catastrophic for beta-cell
374 function. Our present use of an siRNA knockdown model allowed us to better parse the
375 consequences of chronic VPS41-induced insulin deficiency in the beta-cell and acute VPS41
376 loss-of-function. Where no defects in glucose-stimulated insulin secretion was observed with
377 >80% VPS41 protein depletion at 24 hours post-siRNA treatment, total insulin content was
378 significantly reduced, demonstrating a potential disconnect between VPS41's role in these two
379 functions. This may be attributed to preferential siRNA-mediated depletion of the HOPS-
380 associated VPS41 pool, analogous to that observed in VPS39 KO cells, though this is not
381 confirmed. Interestingly, re-expression of a single nucleotide polymorphism of VPS41 (S284P)
382 corresponding to a clinically relevant human VPS41 variant (S285P, [17]) in VPS41 KO INS1
383 cells was sufficient to improve both insulin secretion and content levels without rescuing HOPS
384 function[20]. Where, and how, this HOPS-independent pool of VPS41 contributes to insulin
385 granule biogenesis and exocytosis remain unanswered questions.

386 To our knowledge, such sudden loss of insulin content within hours of a single protein's
387 depletion has not been previously observed. Strikingly, we find that even partial depletion of
388 VPS41 seemingly prompts negative feedback that suggests downregulation of proinsulin
389 translation (Figure 6C) and may eventually result in an insulin secretory defect. This is most
390 strongly evidenced by age-dependent loss of insulin in VPS41KO mice (Figure 2E) and is
391 particularly noteworthy as a recent study reports VPS41 mRNA translation is downregulated

392 in mouse pancreatic beta-cells under chronic hyperglycaemia[32]. Interestingly, as VPS41 KD
393 cells exhibit a similar phenotype to nutrient-starved cells with mTORC1 inhibition coupled
394 with TFE3 nuclear localisation, it is conceivable that TFE3-driven modulation of master
395 regulator Pdx1 is downregulating insulin transcription[33]. *Pdx1* expression is essential for
396 both the cellular development of insulin-positive beta-cells and maintenance of beta-cell
397 identity[34]. It is also appreciated that consistent proinsulin production is necessary for
398 maintenance of beta-cell identity; dual *Ins1* and *Ins2* genetic KO mice develop proinsulin
399 processing defects that cannot be rescued with insulin gene re-expression[35], which we
400 similarly observed in our attempts to re-express proinsulin in VPS41 KO INS1 cells (Figure
401 1E). Ultimately, we find that VPS41 deletion generates a chronically insulin-deficient beta-cell
402 that eventually undergoes a dedifferentiation phenotype. This is replicated *in vivo*, manifesting
403 as a persistent and worsening hyperglycaemia with age, especially in male mice.

404 **Impaired autophagy concurrent with insulin degradation in the beta-cell.** Though VPS41
405 mutant S284P re-expression evidenced a HOPS-independent role for VPS41 in beta-cells, it is
406 apparent from our present study of acute VPS41 depletion that the first and primary defect is
407 the rapid degradation of mature insulin. Insulin granule turnover is critical to beta-cell function,
408 both to replenish secreted insulin, but also to maintain relatively young granules stores; aged
409 insulin granules are less mobile than their younger counterparts[36], less likely to be
410 secreted[23], are more commonly observed within degradative compartments in beta-cells[36].

411 Indeed, our observations of increased SQSTM1 protein in VPS41KD cells likely reflects the
412 build-up of autophagosomes or autophagosome-destined structures within the canonical
413 macroautophagy pathway. Evidence from VPS41KO PC12 neuroendocrine cells[17] and
414 VPS41KO INS1 cells (Supplementary Figure 1A) allow us to surmise that loss of the HOPS
415 complex contributes to autophagolysosomal delay/stall and it is unlikely insulin is degraded
416 through this pathway. This VPS41-mediated autophagic stall has also been observed in non-

417 secretory cells[37]. In beta-cell specific Atg7 KO mice in which autophagy is impaired, serum
418 insulin is reduced[38], with proinsulin observed to colocalize with SQSTM1 in beta-cells[39].
419 Moreover, these cells are more susceptible to ER-stress, which is congruous with our findings
420 in VPS41KO mice (Figure 5). Similarly, in islets from Rab3A KO mice, increased crinophagy,
421 macroautophagy, and microautophagy were all observed in response to impaired exocytosis[7].
422 However, this occurred alongside downregulation of LAMP2 and a significant decrease in
423 proinsulin content – neither of which we observed in our own VPS41 models. Indeed,
424 macroautophagy is generally accepted to be a protective pathway for (pro)insulin content and
425 beta-cell mass[40], and it is suggested that macroautophagy is more likely the primary
426 degradation pathway for *proinsulin* regulation in beta-cells[39].

427 It is conceivable that acute VPS41-dependent disruption of HOPS in the autophagolysosomal
428 pathway impairs normal proinsulin degradation in canonical macroautophagy and in response,
429 the beta-cell upregulates alternate insulin granule degradation pathways such as crinophagy in
430 an attempt to balance the synthesis/storage/degradation axis of insulin granule turnover.
431 Finally, starvation-induced autophagy is also uniquely regulated in pancreatic beta-cells, in
432 which conventional macroautophagy pathways are avoided due to their potential to trigger
433 undesirable stimulation of insulin secretion[9]. As such, starvation- or stress-triggered
434 autophagy (SINGD) has also been well-described to occur through direct immature insulin
435 granule fusion with the lysosome[8]. Considering the mTORC1/TFE3 phenotype mimicking
436 nutrient starvation, it is possible that SINGD may also contribute to the loss of insulin granule
437 content in VPS41 depletion. Crucially, we found that pre-treatment with either lysosome
438 inhibitor chloroquine, or cysteine protease inhibitor E64D was able to rescue insulin content in
439 VPS41KD cells. Interestingly, reductions in total proinsulin and insulin content in chloroquine
440 treatment of INS1 cells measured by ELISA (Figure 6G) were not observed by western blot
441 but may correspond to chloroquine-mediated downregulation of proinsulin synthesis[41].

442 Nonetheless, these data confirm the rapid mature insulin degradation was occurring through
443 lysosomal compartments. It is therefore likely that either microautophagy or crinophagy – that
444 is, direct delivery of insulin granules or insulin granule contents to the lysosome – may be
445 erroneously triggered in the absence of VPS41.

446 Altogether, our data substantiate the critical nature of VPS41 for insulin granule maintenance,
447 and by association, expose a HOPS-dependent role in insulin granule turnover. We also identify
448 a potential VPS41-dependent link to Pdx1 and demonstrate a cellular rewiring of beta-cells in
449 the chronic absence of VPS41. More broadly, we highlight the finely tuned balance between
450 insulin storage and degradation in the beta-cell and its necessity for whole body homeostasis.

451 **Acknowledgements**

452 We would like to thank Elizabeth Lawfull and Jane Calderwood from Australian BioResources
453 (Garvan Institute for Medical Research) for their assistance with mouse ovariectomy
454 procedures, Dr. Ben Crossett (SydneyMS, University of Sydney) with the processing and run
455 of VPS41KO/KD INS1 cell LC-MS/MS samples, and Dr. Ross Laybutt for IRE1-alpha and
456 CHOP antibodies.

457 **Author Contributions**

458 Conceptualization, MAK, CSA; Methodology, MAK, BY, CSA; Validation, YA, BY; Formal
459 Analysis, BY, YA; Investigation, BY, YA, CB, MG, PS, GV, ML; Resources, MAK, Data
460 Curation, BY, YA; Writing – Original Draft, BY; Writing – Review & Editing, BY, YS, CSA,
461 MAK; Visualization, BY; Supervision, MAK; Project Administration, MAK, BY; Funding
462 Acquisition, MAK. MAK is the guarantor of this work and having access to the data of this
463 study, takes responsibility for the contents of this article.

464 **Conflict of Interest Statement**

465 The authors declare no conflict of interests relevant to this article.

---

466 **Figure Legends**

467 **Figure 1. Chronic VPS41 deletion in VPS41KO INS1 cells results in loss of beta-cell**
468 **identity.** Proteomics analysis of VPS41KO INS1 cells compared to WT INS1 control cells
469 identified 1100 significantly differentially expressed proteins **(A)**, from which Gene Ontology
470 pathway enrichment was performed **(B)**. Protein expression levels of key insulin secretory
471 pathway-associated genes **(C)** and beta-cell 'disallowed genes' **(D)** were extracted from the
472 proteomics data to highlight their comparisons. Transfection of proinsulin-GFP into VPS41KO
473 INS1 (and control WT INS1) cells was performed unsuccessfully to rescue proinsulin
474 expression **(E)**.

475 **Figure 2. Islet proteomics of VPS41 beta-cell specific KO female mice at 6 and 16 weeks**
476 **of age.** Blood glucose levels of female Ins1-Cre control (CTRL), VPS41 beta-cell specific
477 heterozygous (VPS41HET) and VPS41 beta-cell specific knockout (VPS41KO) mice at 6 and
478 16 weeks of age **(A)**. Proteomic analysis of VPS41HET and VPS41KO female mice at 6 and
479 16 weeks of age identified 6818 and 7133 proteins respectively, with differentially expressed
480 proteins representing 11% and 43% of the total respective proteome **(B)**. Gene Ontology
481 pathway enrichment was performed on upregulated and downregulated protein sets and
482 compared between 6 and 16 week old mice **(C)**. Protein expression levels of key insulin
483 granule, protein degradation and trafficking-associated genes were extracted from the
484 proteomics data to highlight the HET/KO comparisons at 16 weeks **(D)**. Comparison of protein
485 expression of INS1, INS2 and PDX1 in 6 and 16 week old female mice **(E)**. *$p < 0.05$, ***$p <$
486 0.001, ****$p < 0.0001$ by paired t-test or one-way ANOVA.

487 **Figure 3. Acute VPS41 depletion in INS1 cells by siRNA-mediated knockdown results in**
488 **diminished insulin content.** Protein expression of VPS41, insulin, chromogranin A, Lamp1,

489 Rab5 and beta-actin after siRNA-mediated knockdown of VPS41 (50pmol) and non-targeting
490 control (NTC) siRNA over a 72 hour timecourse **(A)**. VPS41 **(B)** and insulin **(C)** protein
491 expression relative to beta-actin loading control, expressed normalised to NTC siRNA, 48
492 hours post-siRNA-mediated KD of VPS41 (50pmol) in INS1 cells. Insulin expression as
493 measured by fluorescence intensity at 48 hours post-siRNA-mediated knockdown of VPS41
494 and NTC **(D)**. Proteomics analysis of VPS41KD cells at 72 h post-transfection identified 1677
495 differentially expressed proteins **(E)**, from which Gene Ontology pathway enriched was
496 performed **(F)**. Protein expression levels of key autophagy, insulin secretory pathway, and
497 HOPS complex-associated genes were extracted from the proteomics data to highlight these
498 comparisons **(G)**. Glucose-stimulated insulin secretion assay to measure insulin secretion at
499 low (2.8mM) and high (16.7mM) glucose **(H)** and total insulin content normalised to DNA **(I)**
500 in VPS41KD and NTC siRNA control cells at 72 hours post-transfection. Data expressed as
501 mean ± SEM, *$p < 0.05$ by paired t-test.

502 **Figure 4. Whole body and *ex vivo* islet phenotyping comparisons in male and female**
503 **VPS41KO mice.** Total, lean and fat mass **(A)**, fasting blood glucose **(B)** and fasting blood
504 insulins **(C)** in male and female VPS41KO and VPS41HET (control) mice at 7 weeks of age.
505 Plasma insulin **(D)** and glucose measurements **(E)** from male and female VPS41KO and
506 VPS41HET mice during oral glucose tolerance testing. Area under curve **(F)**, glucose
507 measurements expressed as a percent of fasting glucose **(G)** and incremental area under the
508 curve **(H)** of oral glucose tolerance test curves from male and female VPS41KO and
509 VPS41HET mice at 7 weeks age. *Ex vivo* glucose-stimulated insulin secretion assay to measure
510 insulin secretion at low (2.8mM) and high (16.7mM) glucose **(I)**, total insulin content per islet
511 **(J)** and insulin secretion expressed relative to total insulin content **(K)** in male and female
512 VPS41KO and VPS41HET mice. Immunofluorescent staining of insulin in paraffin-embedded
513 pancreatic islet slices of male and female VPS41KO and VPS41HET mice **(L)**. Blood glucose

514 levels of 8 week old female VPS41KO and VPS41HET mice subject to sham or ovariectomy
515 procedure at 5 weeks age **(M)**. Data expressed as mean ± SEM, **p < 0.01, ***p < 0.001,
516 ****p < 0.0001, ns = non-significant by one-way ANOVA.

517 **Figure 5. Expression of ER-stress and autophagy-associated proteins in male and female**
518 **VPS41KO mice.** Representative western blot **(A)** and quantitative expression **(B)** of VPS41,
519 autophagy-associated, and ER-stress-associated proteins in *ex vivo* pancreatic islets from male
520 and female VPS41KO and VPS41HET mice at 7 weeks age. Data expressed as mean ± SEM,
521 ***p < 0.001 by one-way ANOVA.

522 **Figure 6. Alterations to degradation pathways in acute VPS41KD INS1 cells.**
523 Representative immunofluorescent images and quantification of TFE3 **(A)** and mTORC1 and
524 lysotracker **(B)** colocalisation in INS1 cells 24 hours post-transfection with VPS41 or NTC
525 siRNA. Protein expression of VPS41, proinsulin, and beta-actin at 24, 48 and 72 h post-siRNA-
526 mediated VPS41 or NTC knockdown in INS1 cells **(C)**. Immunofluorescent staining of
527 proinsulin in INS1 cells 24 hours post-transfection with VPS41 or NTC siRNA. **(D)**. Insulin
528 measured by ELISA in the media of INS1 cells 24 hours post-transfection with VPS41 or NTC
529 siRNA **(E)**. Representative western blot and quantified insulin expression by immunoblotting
530 in INS1 cells pre-treated for 18 hours with DMSO, 2μM chloroquine or 2μM E64D, 24 hours
531 post-transfection with VPS41 or NTC siRNA **(F)**. Quantified insulin content by ELISA in INS1
532 cells pre-treated for 24 hours with DMSO, 2μM chloroquine or 2μM E64D, 24 hours post-
533 transfection with VPS41 or NTC siRNA **(G)**. Data expressed as mean ± SEM, *p < 0.05, **p
534 < 0.01, ***p < 0.001 by paired t-test or one-way ANOVA.

535 **Supplemental Figure 1.** Expression of mCherry-eGFP-LC3 in VPS41KO and HA-VPS41
536 INS1 cells **(A)**. Quantified insulin protein expression by western blot relative to beta-actin in
537 VPS41KD cells pre-treated with 2 μM chloroquine, 10 μM MG132, 2μM E64D and 1mM

538 ammonium chloride for 24 hours prior to siRNA-mediated knockdown of VPS41 and NTC

539 **(B)**.

540

541

542 1. Yau, B., et al., *Targeting the insulin granule for modulation of insulin exocytosis.* Biochem
543 Pharmacol, 2021. **194**: p. 114821.
544 2. Schnell, A.H., I. Swenne, and L.A. Borg, *Lysosomes and pancreatic islet function. A quantitative*
545 *estimation of crinophagy in the mouse pancreatic B-cell.* Cell Tissue Res, 1988. **252**(1): p. 9-15.
546 3. Vasiljević, J., et al., *The making of insulin in health and disease.* Diabetologia, 2020. **63**(10): p.
547 1981-1989.
548 4. Boland, B.B., C.J. Rhodes, and J.S. Grimsby, *The dynamic plasticity of insulin production in β-*
549 *cells.* Mol Metab, 2017. **6**(9): p. 958-973.
550 5. Lee, Y.H., et al., *β-cell autophagy: Mechanism and role in β-cell dysfunction.* Mol Metab, 2019.
551 **27s**(Suppl): p. S92-s103.
552 6. Pearson, G.L., et al., *A Selective Look at Autophagy in Pancreatic β-Cells.* Diabetes, 2021. **70**(6):
553 p. 1229-1241.
554 7. Marsh, B.J., et al., *Regulated autophagy controls hormone content in secretory-deficient*
555 *pancreatic endocrine beta-cells.* Mol Endocrinol, 2007. **21**(9): p. 2255-69.
556 8. Pasquier, A., et al., *Lysosomal degradation of newly formed insulin granules contributes to β*
557 *cell failure in diabetes.* Nat Commun, 2019. **10**(1): p. 3312.
558 9. Goginashvili, A., et al., *Insulin granules. Insulin secretory granules control autophagy in*
559 *pancreatic β cells.* Science, 2015. **347**(6224): p. 878-82.
560 10. Shvarev, D., et al., *Structure of the HOPS tethering complex, a lysosomal membrane fusion*
561 *machinery.* Elife, 2022. **11**.
562 11. Pols, M.S., et al., *hVps41 and VAMP7 function in direct TGN to late endosome transport of*
563 *lysosomal membrane proteins.* Nat Commun, 2013. **4**: p. 1361.
564 12. van der Beek, J., et al., *CORVET, CHEVI and HOPS - multisubunit tethers of the endo-lysosomal*
565 *system in health and disease.* J Cell Sci, 2019. **132**(10).

566 13. Lin, X., et al., *RILP interacts with HOPS complex via VPS41 subunit to regulate endocytic*
567 *trafficking.* Sci Rep, 2014. **4**: p. 7282.
568 14. Asensio, C.S., et al., *Self-assembly of VPS41 promotes sorting required for biogenesis of the*
569 *regulated secretory pathway.* Dev Cell, 2013. **27**(4): p. 425-37.
570 15. Schoppe, J., et al., *AP-3 vesicle uncoating occurs after HOPS-dependent vacuole tethering.*
571 Embo j, 2020. **39**(20): p. e105117.
572 16. Jiang, D., et al., *Arabidopsis HOPS subunit VPS41 carries out plant-specific roles in vacuolar*
573 *transport and vegetative growth.* Plant Physiol, 2022. **189**(3): p. 1416-1434.
574 17. van der Welle, R.E.N., et al., *Neurodegenerative VPS41 variants inhibit HOPS function and*
575 *mTORC1-dependent TFEB/TFE3 regulation.* EMBO Mol Med, 2021. **13**(5): p. e13258.
576 18. Sanderson, L.E., et al., *Bi-allelic variants in HOPS complex subunit VPS41 cause cerebellar*
577 *ataxia and abnormal membrane trafficking.* Brain, 2021. **144**(3): p. 769-780.
578 19. Steel, D., et al., *Loss-of-Function Variants in HOPS Complex Genes VPS16 and VPS41 Cause*
579 *Early Onset Dystonia Associated with Lysosomal Abnormalities.* Ann Neurol, 2020. **88**(5): p.
580 867-877.
581 20. Burns, C.H., et al., *Pancreatic β-Cell-Specific Deletion of VPS41 Causes Diabetes Due to Defects*
582 *in Insulin Secretion.* Diabetes, 2021. **70**(2): p. 436-448.
583 21. Harney, D.J., et al., *Dietary restriction induces a sexually dimorphic type I interferon response*
584 *in mice with gene-environment interactions.* Cell Rep, 2023. **42**(6): p. 112559.
585 22. Yau, B., et al., *Proteomic pathways to metabolic disease and type 2 diabetes in the pancreatic*
586 *islet.* iScience, 2021. **24**(10): p. 103099.
587 23. Yau, B., et al., *A fluorescent timer reporter enables sorting of insulin secretory granules by age.*
588 J Biol Chem, 2020. **295**(27): p. 8901-8911.
589 24. Okita, N., et al., *Modified Western blotting for insulin and other diabetes-associated peptide*
590 *hormones.* Sci Rep, 2017. **7**(1): p. 6949.

591 25. Schuit, F., et al., *β-cell-specific gene repression: a mechanism to protect against inappropriate*
592 *or maladjusted insulin secretion?* Diabetes, 2012. **61**(5): p. 969-75.
593 26. Brownrigg, G.P., et al., *Sex differences in islet stress responses support female β cell resilience.*
594 Mol Metab, 2023. **69**: p. 101678.
595 27. Jo, S., et al., *Sex Differences in Pancreatic β-Cell Physiology and Glucose Homeostasis in*
596 *C57BL/6J Mice.* J Endocr Soc, 2023. **7**(9): p. bvad099.
597 28. Le May, C., et al., *Estrogens protect pancreatic beta-cells from apoptosis and prevent insulin-*
598 *deficient diabetes mellitus in mice.* Proc Natl Acad Sci U S A, 2006. **103**(24): p. 9232-7.
599 29. Tramunt, B., et al., *Sex differences in metabolic regulation and diabetes susceptibility.*
600 Diabetologia, 2020. **63**(3): p. 453-461.
601 30. Bartolome, A., C. Guillen, and M. Benito, *Autophagy plays a protective role in endoplasmic*
602 *reticulum stress-mediated pancreatic β cell death.* Autophagy, 2012. **8**(12): p. 1757-68.
603 31. Quan, W., Y.M. Lim, and M.S. Lee, *Role of autophagy in diabetes and endoplasmic reticulum*
604 *stress of pancreatic β-cells.* Exp Mol Med, 2012. **44**(2): p. 81-8.
605 32. Cheruiyot, A., et al., *Sustained hyperglycemia specifically targets translation of mRNAs for*
606 *insulin secretion.* J Clin Invest, 2023. **134**(3).
607 33. Pasquier, A., et al., *TFEB and TFE3 control glucose homeostasis by regulating insulin gene*
608 *expression.* Embo j, 2023. **42**(21): p. e113928.
609 34. Gao, T., et al., *Pdx1 maintains β cell identity and function by repressing an α cell program.* Cell
610 Metab, 2014. **19**(2): p. 259-71.
611 35. Ramzy, A., et al., *Insulin Null β-cells Have a Prohormone Processing Defect That Is Not Reversed*
612 *by AAV Rescue of Proinsulin Expression.* Endocrinology, 2022. **163**(6).
613 36. Hoboth, P., et al., *Aged insulin granules display reduced microtubule-dependent mobility and*
614 *are disposed within actin-positive multigranular bodies.* Proc Natl Acad Sci U S A, 2015. **112**(7):
615 p. E667-76.

616 37. Wang, T., et al., *VPS41-mediated incomplete autophagy aggravates cadmium-induced*
617 *apoptosis in mouse hepatocytes.* J Hazard Mater, 2023. **459**: p. 132243.
618 38. Jung, H.S., et al., *Loss of autophagy diminishes pancreatic beta cell mass and function with*
619 *resultant hyperglycemia.* Cell Metab, 2008. **8**(4): p. 318-24.
620 39. Riahi, Y., et al., *Autophagy is a major regulator of beta cell insulin homeostasis.* Diabetologia,
621 2016. **59**(7): p. 1480-1491.
622 40. Sheng, Q., et al., *Autophagy protects pancreatic beta cell mass and function in the setting of a*
623 *high-fat and high-glucose diet.* Sci Rep, 2017. **7**(1): p. 16348.
624 41. Chatterjee, A.K. and H. Schatz, *Effect of chloroquine on biosynthesis, release and degradation*
625 *of insulin in isolated islets of rat pancreas.* Diabetes Res Clin Pract, 1988. **5**(1): p. 9-15.

626

Figure 1

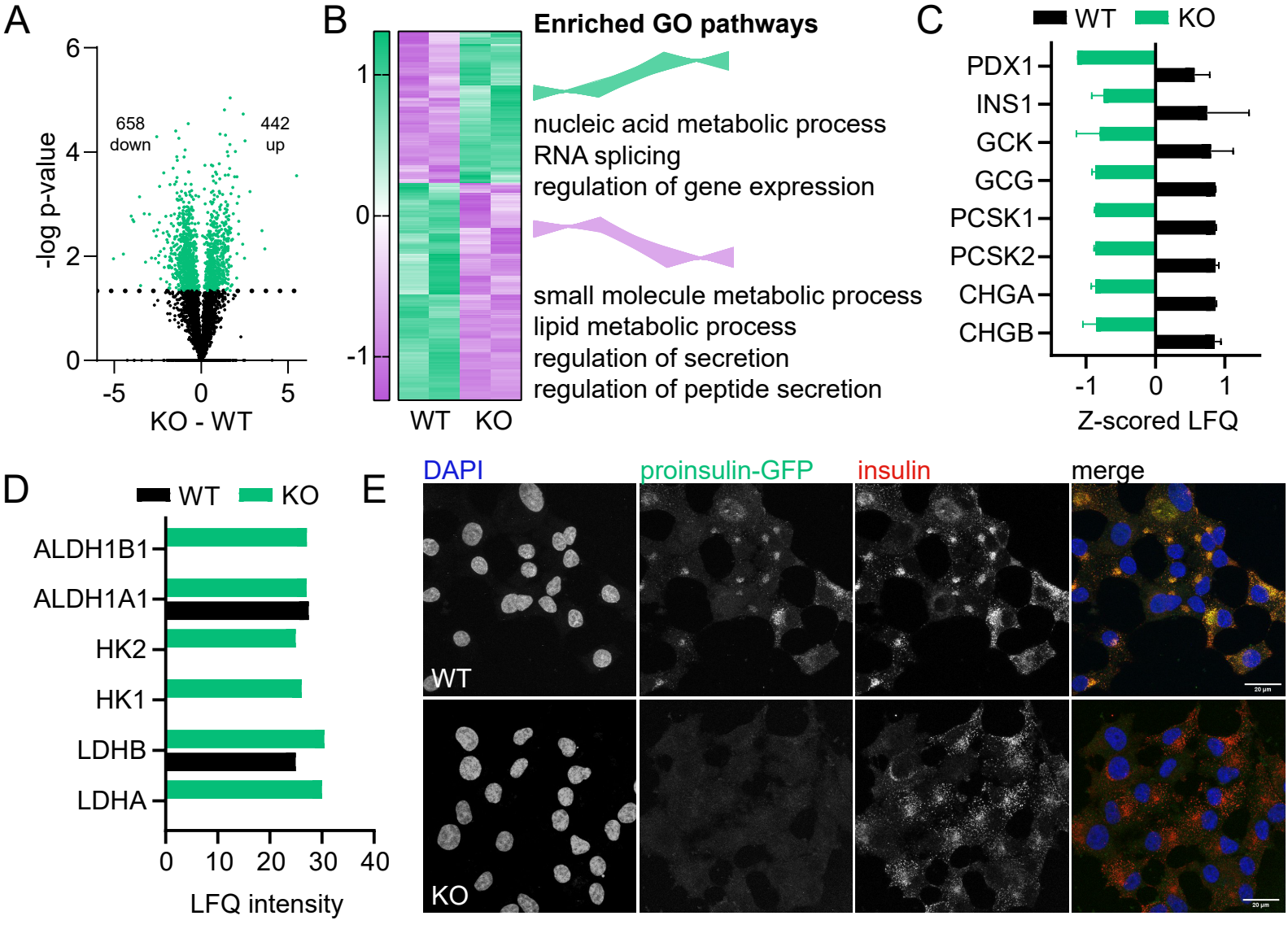
A
658
down
442
up
-log p-value
KO - WT
B
WT
KO
Enriched GO pathways
nucleic acid metabolic process
RNA splicing
regulation of gene expression
small molecule metabolic process
lipid metabolic process
regulation of secretion
regulation of peptide secretion
C
WT
KO
PDX1
INS1
GCK
GCG
PCSK1
PCSK2
CHGA
CHGB
Z-scored LFQ
D
WT
KO
ALDH1B1
ALDH1A1
HK2
HK1
LDHB
LDHA
LFQ intensity
E
DAPI
proinsulin-GFP
insulin
merge
WT
KO

Figure 2

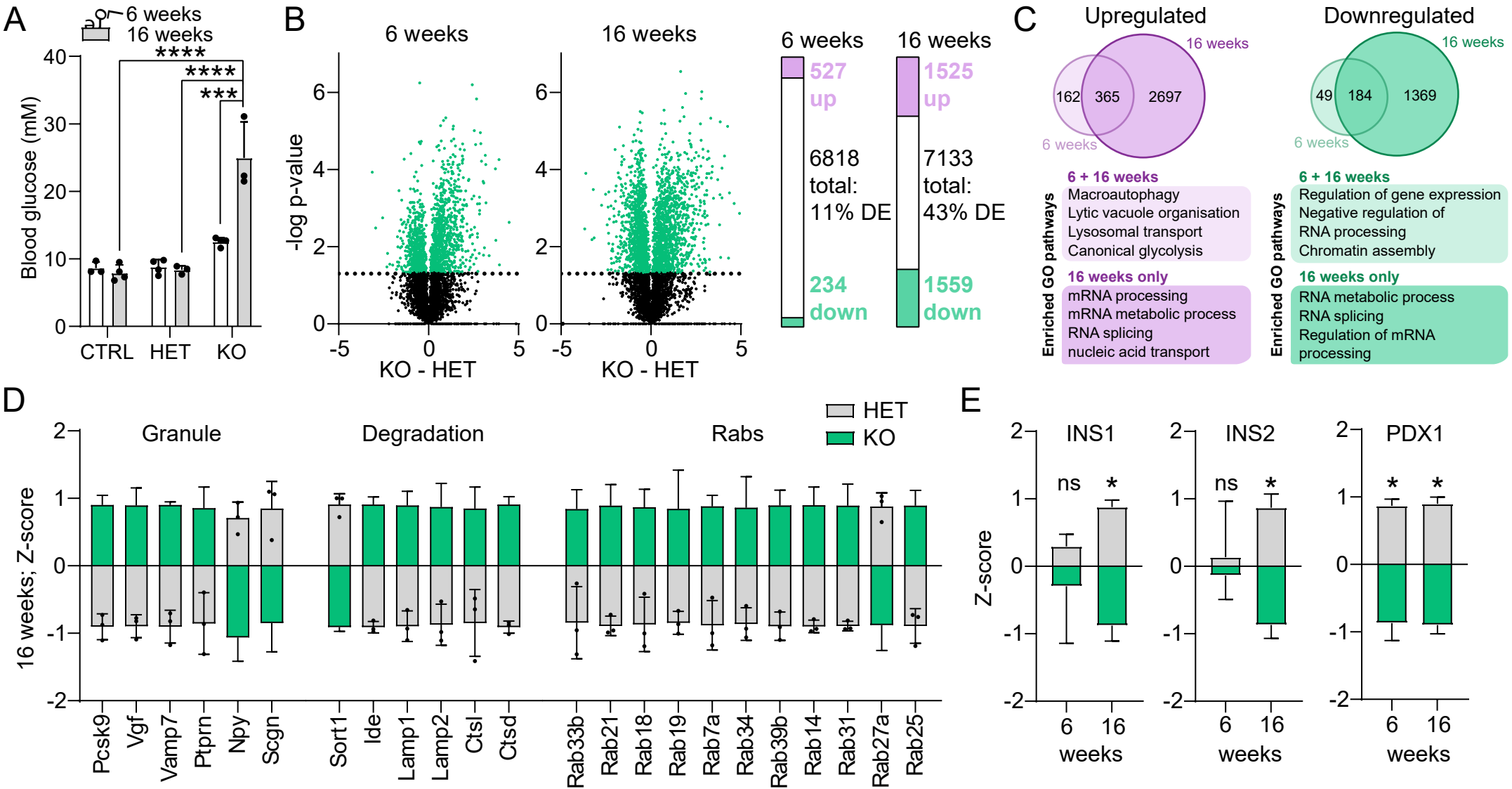
A
6 weeks
16 weeks
Blood glucose (mM)
CTRL
HET
KO
B
6 weeks
16 weeks
-log p-value
KO - HET
6 weeks
16 weeks
527 up
6818 total: 11% DE
234 down
1525 up
7133 total: 43% DE
1559 down
C
Upregulated
Downregulated
162
365
2697
49
184
1369
Enriched GO pathways
6 + 16 weeks
Macroautophagy
Lytic vacuole organisation
Lysosomal transport
Canonical glycolysis
16 weeks only
mRNA processing
mRNA metabolic process
RNA splicing
nucleic acid transport
Regulation of gene expression
Negative regulation of RNA processing
Chromatin assembly
RNA metabolic process
RNA splicing
Regulation of mRNA processing
D
Granule
Degradation
Rabs
HET
KO
16 weeks; Z-score
Pcsk9
Vgf
Vamp7
Ptprn
Npy
Scgn
Sort1
Ide
Lamp1
Lamp2
Ctsl
Ctsd
Rab33b
Rab21
Rab18
Rab19
Rab7a
Rab34
Rab39b
Rab14
Rab31
Rab27a
Rab25
E
INS1
INS2
PDX1
Z-score
ns
weeks

Figure 3

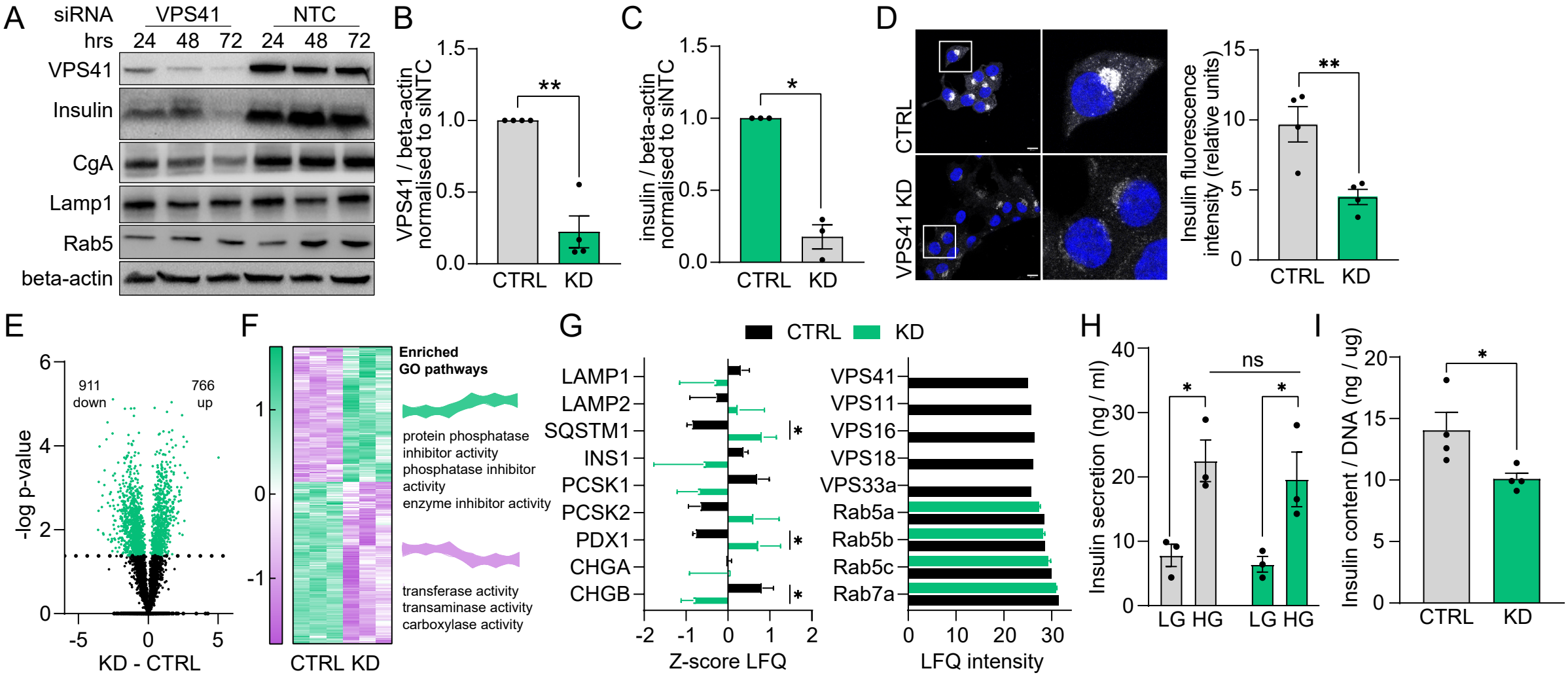
A
siRNA
VPS41
NTC
hrs
24 48 72 24 48 72
VPS41
Insulin
CgA
Lamp1
Rab5
beta-actin
B
VPS41 / beta-actin normalised to siNTC
1.5
1.0
0.5
0.0
**
CTRL KD
C
insulin / beta-actin normalised to siNTC
1.5
1.0
0.5
0.0
*
CTRL KD
D
CTRL
VPS41 KD
Insulin fluorescence intensity (relative units)
15
10
5
0
**
CTRL KD
E
-log p-value
6
4
2
0
911 down
766 up
-5 0 5
KD - CTRL
F
1
0
-1
CTRL KD
Enriched GO pathways
protein phosphatase inhibitor activity
phosphatase inhibitor activity
enzyme inhibitor activity
transferase activity
transaminase activity
carboxylase activity
G
CTRL KD
LAMP1
LAMP2
SQSTM1
INS1
PCSK1
PCSK2
PDX1
CHGA
CHGB
*
*
*
-2 -1 0 1 2
Z-score LFQ
VPS41
VPS11
VPS16
VPS18
VPS33a
Rab5a
Rab5b
Rab5c
Rab7a
0 10 20 30
LFQ intensity
H
Insulin secretion (ng / ml)
40
30
20
10
0
ns
*
*
LG HG LG HG
I
Insulin content / DNA (ng / ug)
20
15
10
5
0
*
CTRL KD

Figure 4

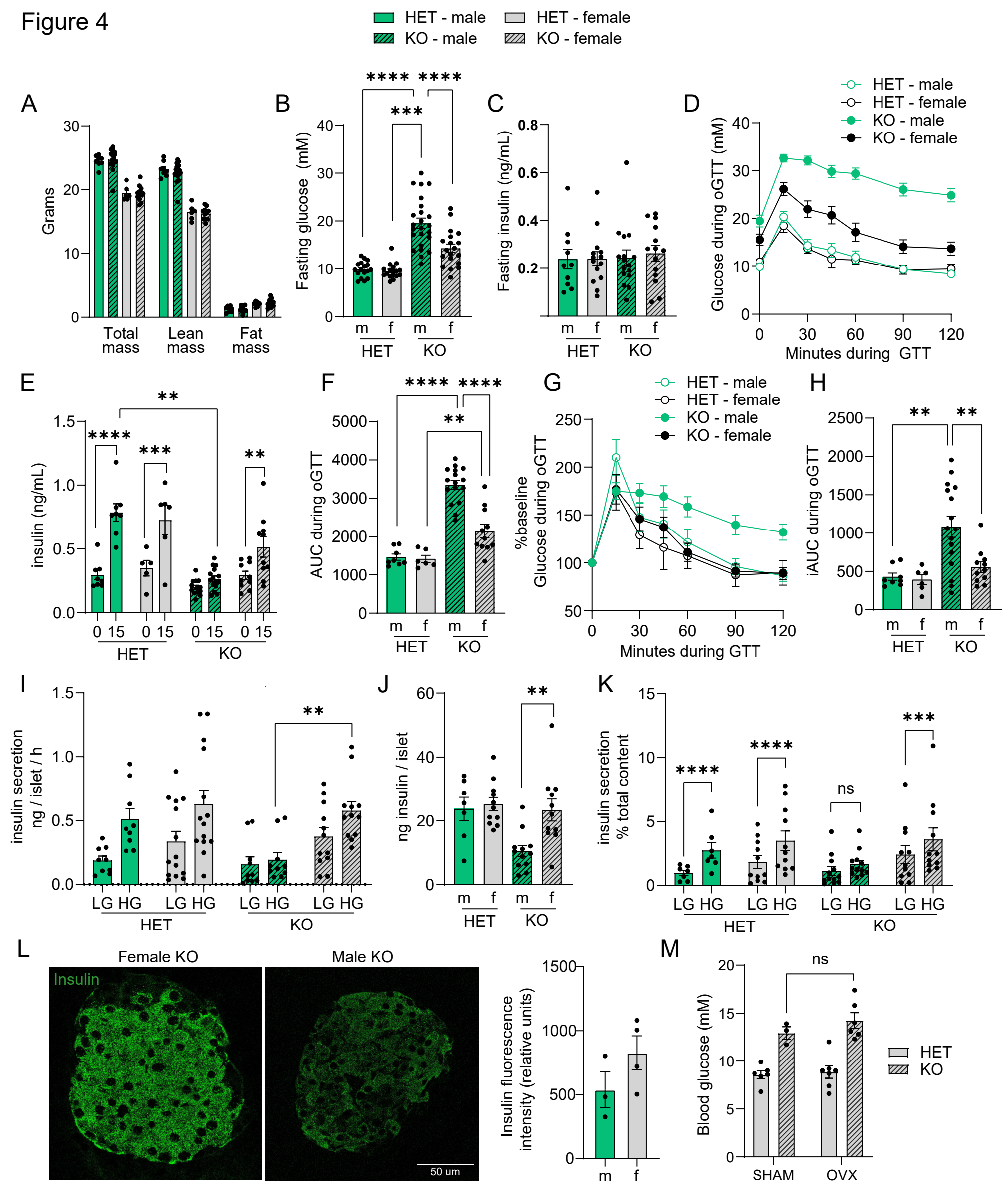
HET - male
KO - male
HET - female
KO - female
A
Grams
Total mass
Lean mass
Fat mass
B
Fasting glucose (mM)
m f m f
HET KO
C
Fasting insulin (ng/mL)
D
Glucose during oGTT (mM)
Minutes during GTT
E
insulin (ng/mL)
0 15 0 15 0 15 0 15
F
AUC during oGTT
G
%baseline Glucose during oGTT
H
iAUC during oGTT
I
insulin secretion ng / islet / h
LG HG LG HG LG HG LG HG
J
ng insulin / islet
K
insulin secretion % total content
ns
L
Female KO
Male KO
Insulin
50 um
Insulin fluorescence intensity (relative units)
M
Blood glucose (mM)
SHAM
OVX

Figure 5

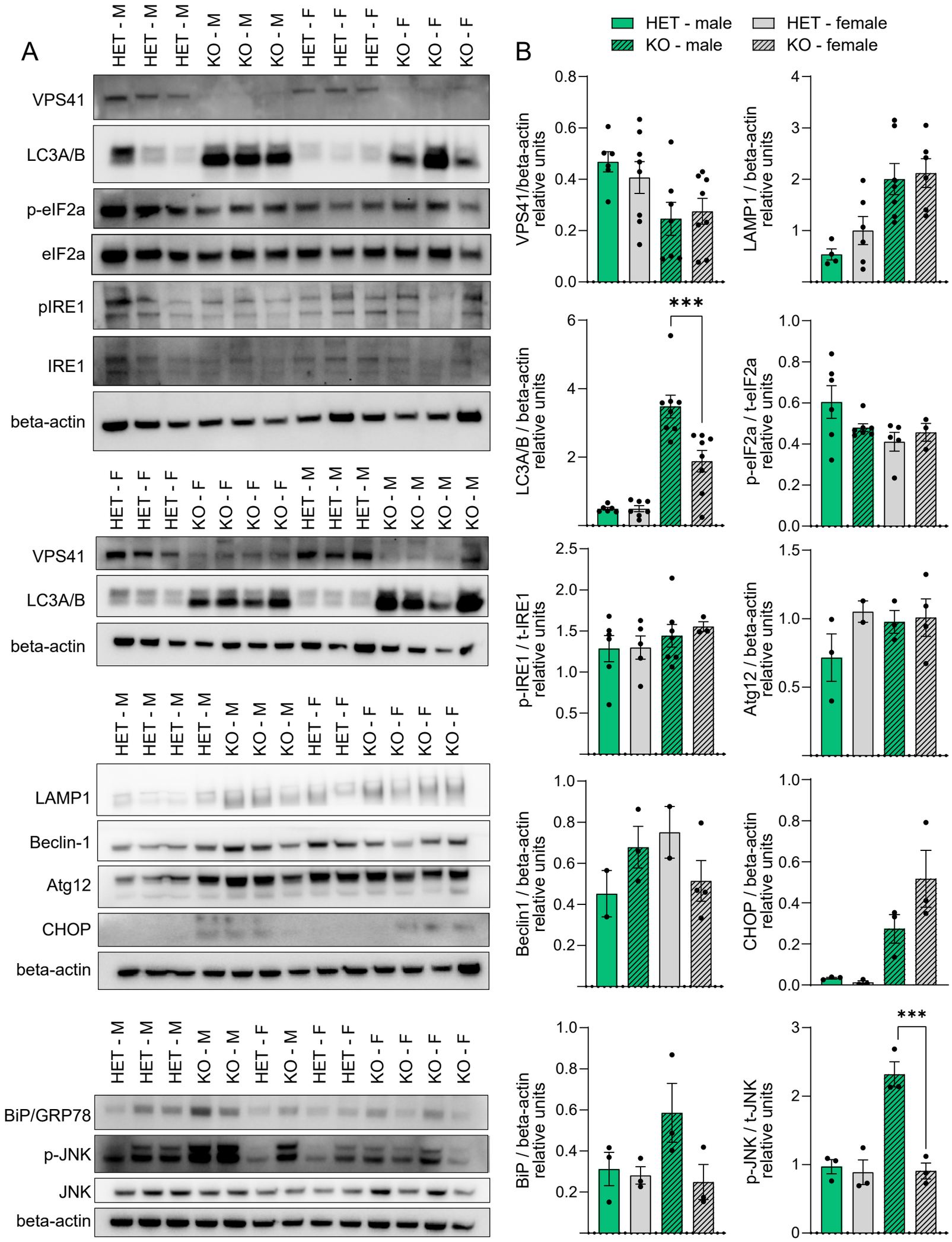
A
HET - M
KO - M
HET - F
KO - F
VPS41
LC3A/B
p-eIF2a
eIF2a
pIRE1
IRE1
beta-actin
LAMP1
Beclin-1
Atg12
CHOP
BiP/GRP78
p-JNK
JNK
B
HET - male
KO - male
HET - female
KO - female
VPS41/beta-actin relative units
LAMP1 / beta-actin relative units
LC3A/B / beta-actin relative units
p-eIF2a / t-eIF2a relative units
p-IRE1 / t-IRE1 relative units
Atg12 / beta-actin relative units
Beclin1 / beta-actin relative units
CHOP / beta-actin relative units
BiP / beta-actin relative units
p-JNK / t-JNK relative units
***
***

Figure 6

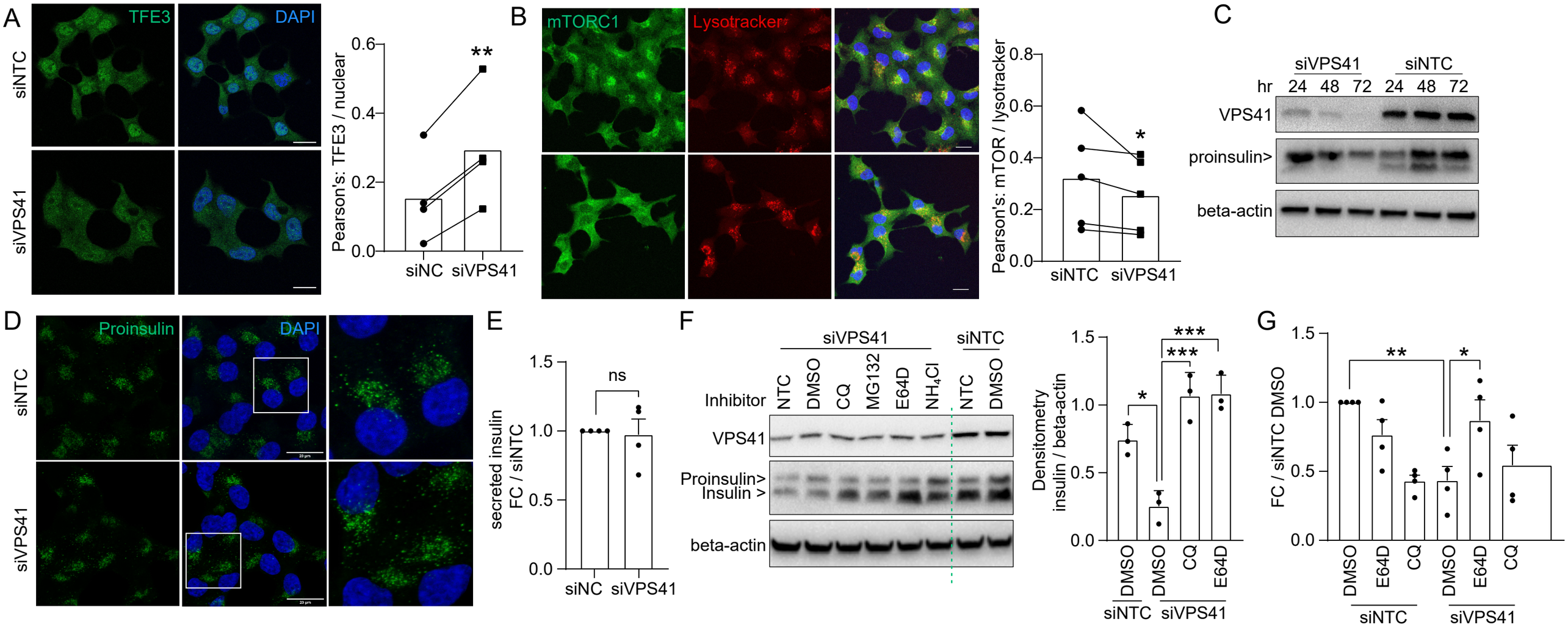
A
TFE3
DAPI
siNTC
siVPS41
Pearson's: TFE3 / nuclear
0.6
0.4
0.2
0.0
**
siNC
siVPS41
B
mTORC1
Lysotracker
Pearson's: mTOR / lysotracker
0.8
0.6
0.4
0.2
0.0
*
siNTC
siVPS41
C
siVPS41
siNTC
hr 24 48 72 24 48 72
VPS41
proinsulin>
beta-actin
D
Proinsulin
DAPI
siNTC
siVPS41
E
secreted insulin
FC / siNTC
1.5
1.0
0.5
0.0
ns
siNC
siVPS41
F
siVPS41
siNTC
Inhibitor
NTC
DMSO
CQ
MG132
E64D
NH4Cl
NTC
DMSO
VPS41
Proinsulin>
Insulin >
beta-actin
Densitometry
insulin / beta-actin
1.5
1.0
0.5
0.0
*
***
***
DMSO
DMSO
CQ
E64D
siNTC
siVPS41
G
FC / siNTC DMSO
1.5
1.0
0.5
0.0
**
*
DMSO
E64D
CQ
DMSO
E64D
CQ
siNTC
siVPS41

Supplementary Figure 1

A

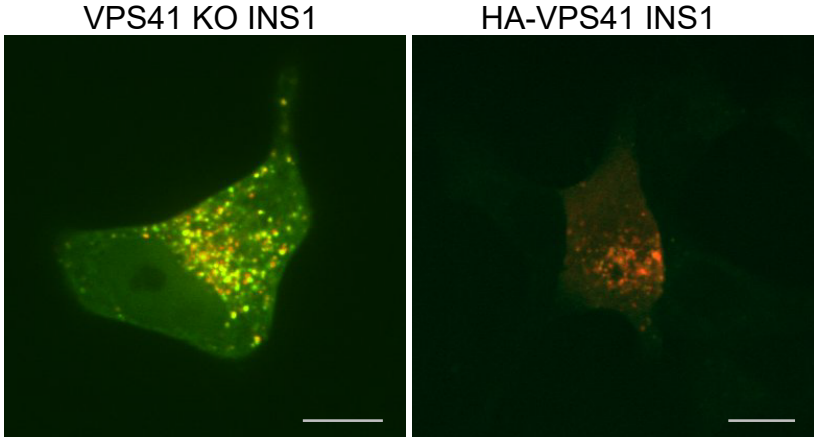

mCherry-eGFP-LC3
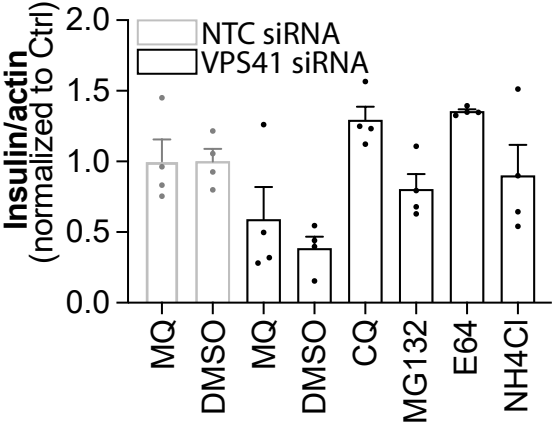
B